Letter Vol. 48, No. 21 / 1 November 2023 / Optics Letters 5767

Optics Letters

Super-long-range distributed vibration sensor based on the polarimetric forward-transmission of light

George Y. Chen,[1,2] Xing Rao,[1,2] Kuan Liu,[1,2] Yuhang Wang,[1,2] Neil G. R. Broderick,[3] Gilberto Brambilla,[4] and Yiping Wang[1,2,*]

[1]Key Laboratory of Optoelectronic Devices and Systems of Ministry of Education and Guangdong Province, College of Physics and Optoelectronic Engineering, Shenzhen University, Shenzhen 518060, China
[2]Shenzhen Key Laboratory of Photonic Devices and Sensing Systems for Internet of Things, Guangdong and Hong Kong Joint Research Centre for Optical Fiber Sensors, Shenzhen University, Shenzhen 518060, China
[3]Dodd Walls Centre for Photonic and Quantum Technologies and the Department of Physics, University of Auckland, Private Bag 92019, Auckland, New Zealand
[4]Optoelectronics Research Centre, University of Southampton, Southampton SO17 1BJ, UK
*ypwang@szu.edu.cn

Received 31 August 2023; revised 4 October 2023; accepted 7 October 2023; posted 9 October 2023; published 30 October 2023

Undersea earthquake-triggered giant tsunamis pose significant threats to coastal areas, spanning thousands of kilometers and affecting populations, ecosystems, and infrastructure. To mitigate their impact, monitoring seismic activity in underwater environments is crucial. In this study, we propose a new, to the best of our knowledge, approach for monitoring vibrations in submarine optical cables. By detecting vibration-induced polarization rotation, our dual-wavelength fiber-optic sensing system enables precise measurement of acoustic/vibration amplitude, frequency, and position. As a proof of concept, a double-ended forward-transmission distributed fiber-optic vibration sensor was demonstrated with a single vibration source with a sensitivity of 3.4 mrad/με at 100 Hz (20 m fiber on PZT), limit of detection of 1.7 pε/Hz$^{1/2}$ at 100 Hz, sensing range of 121.5 km without an optical amplifier, spatial resolution of 5 m, and position error as small as 34 m. The vibration frequency range tested is from 0.01 to 100 Hz. The sensing system has several advantages, including elegant setup, noise mitigation, and super-long sensing distance.

https://doi.org/10.1364/OL.504740

Undersea earthquakes [1] can cause massive tsunamis that can cause irreparable damage to coastal populations, ecosystems, and infrastructure within thousands of kilometers. For example, the tsunami triggered by the massive M9.1 earthquake off the coast of Sumatra (December 26, 2004) [2] caused damage around the Indian Ocean, killing more than 230,000 people. The use of submarine optical cables to remotely monitor a large area of the seabed can provide real-time feedback on changes in the local environment of the seabed caused by marine earthquakes, thereby reducing losses and saving lives. More than 1.2 million km of submarine cable [3] crisscross the seafloor, a hidden infrastructure that makes the Internet possible. If the optical fibers in these undersea cables can be sensitized to detect seismic waves in addition to their normal functions (communication-sensing dual functionality) [4], oceans can be turned into a vast sensor network.

Distributed fiber-optic vibration sensing [5] has been extensively researched in recent years due to its enormous potential in various applications such as structural health monitoring [6], intrusion detection [7], and earthquake monitoring [8]. The most widely used method for achieving distributed vibration sensing is optical time-domain reflectometry (OTDR) [9] of backscattered Rayleigh signal. Conventional sensing methods all employ weak backscattered Rayleigh light signals, which limit the sensing distance to a few tens of kilometers. Furthermore, the high cost of commercial distributed sensors, mostly due to the high-spec laser source, limits their use to long-distance seabed monitoring.

In addition to these well-known solutions [10] that employ backscattered light signals, forward-transmission-type fiber-optic interferometric sensors [10] have also garnered a considerable interest in recent years for distributed vibration measurements due to their unique advantage of super-long sensing distance. Vibration information along the sensing fiber can be obtained by measuring changes in the phase delay or state of polarization (SOP) [11], and the time delay between counter-propagating optical signals can be used for event localization. Up to 10,500 km (repeater-to-repeater span length of 45 to 90 km) using a trans-oceanic submarine cable has been demonstrated. In general, sensing systems with longer sensing distances without optical amplification can reduce the offshore resources and maintenance required. To address the issues of sensing distance and cost, we propose a new type of forward-transmission fiber-optic acoustic/vibration sensor that can achieve a sensing distance of 121.5 km (fixed wavelength, potentially broadband) without an inline optical amplifier after the laser source. The main innovations are the simple yet effective system design involving polarization-rotation-induced power detection along a single fiber and the wavelength diversity design to filter out unwanted Rayleigh and Brillouin backscattered light. Only a sensing fiber is needed, no need for a reference fiber, which

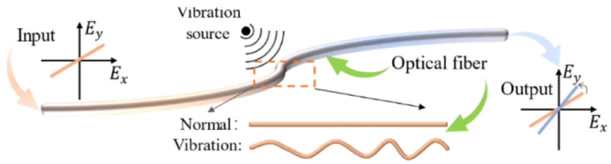

Fig. 1. Polarization-based sensing mechanism.

means that this method can be conveniently adopted by existing optical communication networks based on PolSK demodulation. There is no stringent requirement on a narrow laser linewidth; thus such sensing systems can be built with low cost. By using dual-wavelength and bidirectional operation in single-mode fiber, vibration-induced rotation in the state of polarization is detected in real time, which can resolve vibration signals along the sensing fiber, as well as vibration amplitude and frequency. Through the use of forward-propagating continuous-wave light instead of much weaker Rayleigh backscattered light, the sensing range can be significantly extended. The vibration position can be determined through simple cross correlation between the bidirectional sampled waveforms.

Overall, the new system design enables (a) superior signal-to-noise ratio, unaffected by Rayleigh noise; (b) reduced nonlinear effects; (c) extended sensing distance without amplifiers; (d) maintained vibration positioning and spatial resolution; (e) decoupled resolution and range; and (f) no weak signal regions, unlike double-ended OTDR systems.

Polarization demodulation is a common sensing technique widely used in distributed fiber-optic sensors, such as polarization-OTDR. As depicted in Fig. 1, linearly polarized light is first injected into the sensing fiber. When the optical fiber is undisturbed, there is no compression/bend/twist, resulting in a stable state of polarization (SOP) at the fiber output. However, when an external perturbation such as a vibration is applied, the fiber can be compressed/bent/twisted, causing a change in the output SOP. By detecting the changes in SOP in the form of power modulation, such as rotation angle, ellipticity, or degree of polarization (DOP), we can accurately measure the external perturbations applied to the fiber. This sensing technique has several advantages over other phase-based sensing methods, such as simplicity and low cost. Furthermore, polarization demodulation can be applied to various sensing applications, including temperature, strain, and vibration real-time measurements for structural health monitoring.

To verify the suitability of polarization demodulation for long-range vibration sensing [12], tests were conducted on optical fibers of varying lengths, with a particular interest in the SOP and DOP. As revealed by Fig. 2(a), when there is no vibration, the SOP of the output light from different fiber lengths each represented by a point on the Poincaré sphere remains relatively unchanged. Figure 2(b) shows that as the fiber length increases, the change in the DOP is negligible. In the presence of an external perturbation such as a vibration at 100 Hz, the SOP point traces a curve on the Poincaré sphere and rewinds according to the vibration period, as shown in Fig. 2(c). Meanwhile, the DOP only experiences a slight change, as shown in Fig. 2(d). These results demonstrate that SOP changes can provide an effective measure of vibration signals. Note that the actual polarization angle will change rapidly with time due to a non-zero ellipticity, and thus the detected power ratio represents the envelope of its electric field transformation. Any vibration-induced phase shift would only

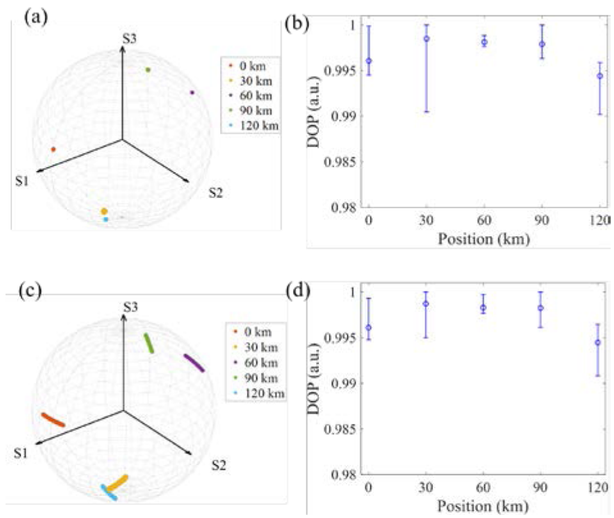

Fig. 2. Vibration-induced changes in polarization. (a) Ambient SOP. (b) Ambient DOP. (c) SOP with 100 Hz vibration. (d) DOP with 100 Hz vibration.

speed up or slow down the rate of SOP rotation but would not affect the steady-state powers observed by the relatively slow photodetectors.

In the experiment, a dual-wavelength laser source (1549.72 nm and 1550.12 nm, 500 kHz linewidth) transmitted forward and backward optical power to talling 2.3 mW. The 121.5 km sensing fiber employed photodetectors and an oscilloscope with 5 GHz bandwidth. Vibration events altered the SOP in both directions, demodulated by a polarization beam-splitter. The signal arrival time difference determines the vibration position. The data was collected at 40 MS/s within 10 ms windows, denoting a 5 m spatial resolution. The spatial resolution is defined as the spatial interval corresponding to the sampling time interval. It also means that the higher the sampling rate, the higher the positioning accuracy. Under laboratory conditions, temperature insulation, and other factors that helped maintain a consistent polarization, vibrations induced polarization modulation in both fiber directions, ensuring similar SOP changes.

To fully understand the working principles of the sensing system, the polarization angle (represents the net angle or integral of all polarization changes) can be obtained by measuring the optical power of X and Y polarizations:

$$I_X = I\cos^2(\theta_0 + \theta_s(t + nZ/c)), \tag{1}$$

$$I_Y = I\sin^2(\theta_0 + \theta_s(t + nZ/c)), \tag{2}$$

where I is the output optical power, θ_0 is the initial polarization angle of light, n is the effective refractive index of the optical fiber, Z is the distance of vibration from the nominal end of the fiber, c is the speed of light in vacuum, and $\theta_s(t + nZ / c)$ is the change in polarization angle caused by the vibration applied to the fiber. When vibration is applied to the section of the optical fiber (the sensing fiber), it changes the local refractive index of the fiber and the SOP of light transmitted in the fiber and ultimately causes a change in the polarization angle of the output light. The vibration event can be detected by monitoring the demodulated polarization angle of the output light. The polarization angle can be obtained by measuring the optical power of

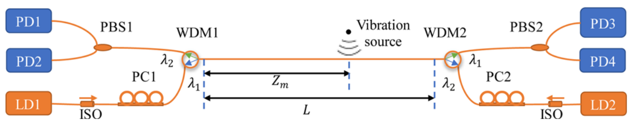

Fig. 3. Experiment setup. λ_1 :1549.72 nm, λ_2:1550.12 nm. ISO, isolator; PBS, polarization beam-splitters; PC, polarization controller; PD, photodetector; WDM, wavelength division multiplexer.

X and Y polarizations:

$$\theta = \text{atan}\left(\sqrt{I_y/I_X}\right). \tag{3}$$

After obtaining θ, the DC component is removed via subtraction of the mean value to obtain the change in polarization angle ($\Delta\theta$) caused by vibration along the sensing fiber. As shown in Fig. 3, along the sensing fiber of length L, the vibration occurs at position Z_m, and the polarization-modulated light propagates in both directions along the fiber. The time delay for the vibration signal to propagate from the vibration location to the two photodetectors is expressed by $t_1 = nZ_m / c$ and $t_2 = n(L - Z_{m)} / c$. Hence, the time delay difference is given by $\Delta t = t_2 - t_1$. The time delay difference between the two ends of the fiber can be obtained by calculating the cross correlation of the two sets of θ data associated with the two propagation directions. Since the two light paths are similar, vibrations applied to the sensing fiber should result in a similar change, and thus their output waveforms should exhibit high correlation. Once Δt is obtained from the correlation results, the vibration location can be determined by:

$$Z_m = (L - c\Delta t/n)/2. \tag{4}$$

Due to the severe Brillouin backscattering that occurs during the long-distance transmission of CW light in the optical fiber, the optical signal becomes swamped with noise. To reduce the effect of Brillouin scattering, we used an experimental system shown in Fig. 3, which utilizes two counter-propagating wavelengths of light. Both wavelengths generate stimulated Brillouin scattering (SBS) that are opposite in direction to the signal light transmission, and SBS causes a shift in the laser wavelength by approximately 100 pm. Therefore, 100 G DWDM technology is employed to achieve narrowband filtering, which effectively filtered out Brillouin backscattered light by wavelength division, leading to a higher SNR.

To evaluate the performance of the sensing system, vibration was applied to a 20 m section of sensing fiber coiled and fixed around a disk-shaped piezoelectric transducer (PZT). The fiber section was centered at an arbitrary position of approximately 50.68 km (i.e., Zm = 50.68 km). The PZT generated continuous vibrations based on a 100 Hz sinc drive signal, which transferred its displacement in the form of strain to the bonded fiber. The measured temporal waveforms at both ends are shown in Fig. 4(a). Similar waveforms can be observed with slight differences in arrival time (for convenience of display, only a single period is shown). The intensity difference in the waveforms is likely attributed to non-identical optical losses along the optical fibers, connectors, and fiber couplers. Note that a periodic sinc function was chosen to represent a vibration shockwave, and a sine function can be used as well.

Due to the high degree of correlation between the measured waveforms from both output ends, complex time–frequency analysis is not needed. The collected data from the photodetectors can be directly used to calculate the cross correlation between the two waveforms; thus the signal time delay can deduce the vibration position. Compared with systems that require time–frequency analysis, the proposed sensing system uses simpler data processing and thus less computation load, which allows detection of higher-frequency vibration signals, as well as more accurate positioning. As an example, when the time delay estimation is 102.5 μs, the vibration position calculated based on Eq. (4) is 50.72 km, which is in close agreement with the true vibration position of 50.68 km. It should be noted that the two signals obtained from the two ends may have a negative correlation depending on the initial polarization angles, and the positioning accuracy is similar in both cases.

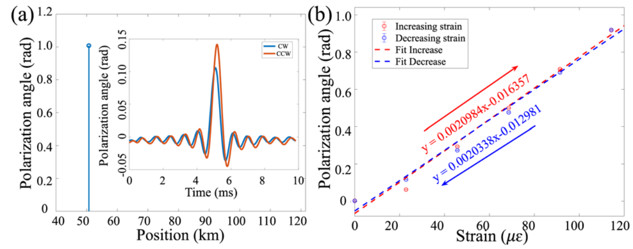

Fig. 4. (a) Vibration positioning based on cross correlation of bidirectional signals. Inset: change in polarization angle of the two optical directions. (b) SOP angle change under different strain conditions at the same position.

After investigating the optical response under different strain, the data reveal a linear relationship between applied strain and polarization angle. As shown in Fig. 4(b), the red line represents the linear fit of gradually increasing strain, and the blue line represents that of gradually decreasing strain. The average gradient (or sensitivity) of the linear fitting is 0.0020984 rad/με and 0.0020338 rad/με for increasing and decreasing strains, respectively. The consistency indicates that the sensor response is reversible, demonstrating the dynamic range as well as the reliability and stability of the sensor. The error bars (typically ±0.001 rad) are due to environment-induced bending and twisting of the optical fiber and the contribution of noise in the photodetectors.

Due to PZT limitations, we cannot test high signal frequencies (over 750 Hz). The one-way transit time of 121.5 km is 0.6075 ms; thus the highest measurable vibration frequency based on one signal period is 1646 Hz, due to the cross correlation ambiguity when more than one signal period is observed within each measurement duration (single-pass transit time of light or maximum arrival time difference between the two detection ends). The trend of increasing sensitivity, shown in Fig. 5(a), with increasing vibration frequency is likely due to the damping effect of the PZT's mechanical structure at relatively low frequencies. The trend of decreasing LoD (limit of detection) with increasing frequency can be attributed to the increase in signal-to-noise ratio at higher frequencies, caused by greater attenuation of ambient vibrations by the optical table and temperature drifts occurring only at relatively low frequencies. The sensitivity and LoD can be improved at lower frequencies by lowering the resonant frequency of the mechanical structure or PZT. Overall, the frequency response characterization provides a valuable insight into the performance of the sensing system in addition to the range of applications.

To ensure that the optical response was comparable even when the vibration occurred at a different position, the sensitivity and LoD were measured at a fixed vibration frequency

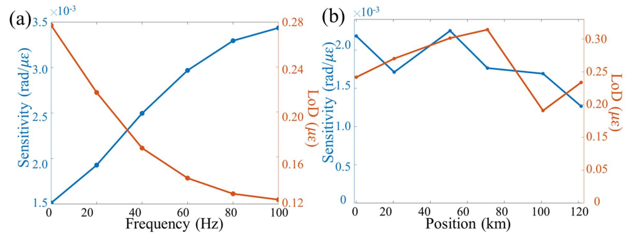

Fig. 5. (a) SOP sensitivity and LoD under different vibration frequencies at the same position. (b) Sensitivity and limit of detection at different vibration positions (100 Hz).

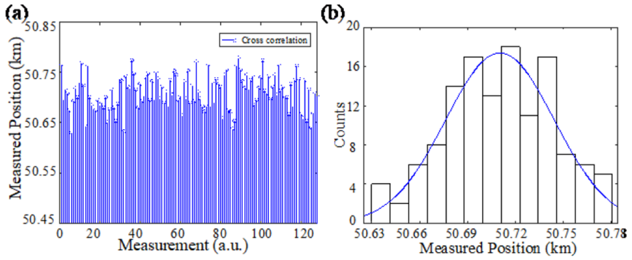

Fig. 6. Repeatability measurements. (a) Experiment results of 128 vibration positioning measurements. (b) Histogram of the probability distribution of the measured position.

of 100 Hz. It was found that the sensitivity fluctuates around 0.002 rad/με and the LoD is on average 220 nε, as shown in Fig. 5(b). The deviations in sensitivity and LoD among different positions are likely caused by inconsistent noise levels during the measurement process. The sensitivity will also change for the slowly varying SOP ellipticity. Practical applications may take into account the slightly varying sensitivity with distance for calibration. Overall, the results demonstrate that the sensing system has a fairly consistent performance independent of the vibration position, which is essential for long-range monitoring.

Repetitive vibration measurements were carried out to study the repeatability of vibration positioning. In total, 128 repeat measurements were performed, and the results of Z_m are plotted in Fig. 6(a). Figure 6(b) shows a histogram of the collective measurement results, revealing a "normal" probability distribution of the measured Z_m. The peak of the Gaussian fitting curve occurs at 50.72 km, which matches that of the actual vibration position derived from the optical fiber manufacturer's specifications. The root mean square (RMS) error of the measured Z_m was also calculated to evaluate the positioning accuracy. Here, N = 128 is the number of measurements, and Z_m is the mean value of the measured Z_m. The RMS error from this dataset is calculated to be 34 m.

To extend the positioning error characterization, different vibration positions were tested. Specifically, the PZT with coiled fiber was deployed at six different distances from one end of the sensing system: 0 km, 20.50 km, 50.68 km, 70.78 km, 101.50 km, and 121.50 km. Overall, the positioning error was within 200 m. The closer the vibration was to the middle of the entire length of the sensing fiber, the smaller the positioning error. This can be explained by symmetry and thus near-equal optical losses. Toward the two ends, the positioning error grew larger. From Table 1, it can be seen that the smallest error occurred at 50.71 km, which is only 34 m. In comparison, the

Table 1. Positioning Error of Different Positions

Position (km)	0.18	20.41	50.71	70.82	101.54	121.55
Error (km)	0.194	0.118	0.034	0.058	0.082	0.173

larger errors at the two ends were 194 m and 173 m. It is likely that the more complex signal comparison methods can improve the accuracy.

The experiment results reveal the potential for the proposed sensing system to be used for seabed event monitoring. Since a typical seabed is a relatively quiet environment, external perturbations from the ambient environment are relatively small, which allows natural events (e.g., undersea earthquake) or man-made events (e.g., fish trawlers) to stand out. In practice, the perturbed fiber section could be much longer than the 20 m shown in the laboratory, possibly reaching hundreds of meters or even several kilometers.

In conclusion, we have experimentally demonstrated a new type of forward-transmission polarization-demodulation vibration sensor based on a WDM configuration, which overcomes the sensing distance limitations caused by Brillouin scattering and coherent Rayleigh backscattering noise. Preliminary results demonstrated a sensitivity of 3.4 mrad/με at 100 Hz, LoD of 1.7 pε/Hz$^{1/2}$ at 100 Hz, sensing range of 121.5 km without an optical amplifier, spatial resolution of 5 m, and position error as small as 34 m. The main innovations are the simple (faster processing and less hardware, but does not retain differential phase information) system design involving polarization-rotation-induced power detection along a single fiber. Single-source vibration monitoring was demonstrated in real time, and future work will focus on real-time multi-vibration-source monitoring. By using forward-transmission continuous-wave light instead of weak backward scattered light, the proposed sensing system can achieve a super-long sensing distance. In addition, by employing polarization demodulation, there is no longer a need for ultra-narrow laser linewidth, which reduces cost.

Funding. Research start-up fund for high-end talent at Shenzhen University.

Disclosures. The authors declare no conflicts of interest.

Data availability. Data underlying the results presented in this paper are not publicly available at this time but may be obtained from the authors upon reasonable request.

REFERENCES

1. W. B. Wu, Z. W. Zhan, S. R. Peng, *et al.*, Science **369**, 1510 (2020).
2. N. Mori, K. Satake, D. Cox, *et al.*, Nat. Rev. Earth Environ. **3**, 557 (2022).
3. G. Marra, D. M. Fairweather, V. Kamalov, *et al.*, Science **376**, 874 (2022).
4. B. M. Howe, M. Angove, J. Aucan, *et al.*, Front. Earth Sci. **9**, 1 (2022).
5. J. Huang, Y. Chen, Q. Song, *et al.*, Opt. Express **28**, 24820 (2020).
6. S. Abedin, A. M. Biondi, R. Wu, *et al.*, Sensors **23**, 1591 (2023).
7. S. Q. Liu, F. H. Yu, R. Hong, *et al.*, Opto-Electron. Adv. **5**, 200078 (2022).
8. Z. Y. Liu, S. Q. Zhang, C. K. Yang, *et al.*, Front. Mar. Sci. **9**, 1 (2022).
9. C. Wang, Y. Shang, X. H. Liu, *et al.*, Opt. Express **23**, 29038 (2015).
10. Z. Zhao, L. Shen, Y. Dang, *et al.*, Opt. Lett. **46**, 3685 (2021).
11. Z. W. Zhan, M. Cantono, V. Kamalov, *et al.*, Science **371**, 931 (2021).
12. A. Mecozzi, M. Cantono, J. C. Castellanos, *et al.*, Optica **8**, 788 (2021).